Monthly Notices
of the
ROYAL ASTRONOMICAL SOCIETY

MNRAS **494,** 1411–1423 (2020)
Advance Access publication 2020 March 24

doi:10.1093/mnras/staa807

A bound on the $^{12}C/^{13}C$ ratio in near-pristine gas with ESPRESSO

Louise Welsh [1]★ Ryan Cooke [1] Michele Fumagalli [1,2,3] and Max Pettini [4]

[1] *Centre for Extragalactic Astronomy, Durham University, South Road, Durham DH1 3LE, UK*
[2] *Institute for Computational Cosmology, Durham University, South Road, Durham DH1 3LE, UK*
[3] *Dipartimento di Fisica G. Occhialini, Università degli Studi di Milano Bicocca, Piazza della Scienza 3, I-20126 Milano, Italy*
[4] *Institute of Astronomy, University of Cambridge, Madingley Road, Cambridge CB3 0HA, UK*

Accepted 2020 March 19. Received 2020 March 13; in original form 2020 January 9

ABSTRACT

Using science verification observations obtained with ESPRESSO at the Very Large Telescope (VLT) in 4UT mode, we report the first bound on the carbon isotope ratio $^{12}C/^{13}C$ of a quiescent, near-pristine damped Lyα (DLA) system at $z = 2.34$. We infer a limit $\log_{10}{}^{12}C/^{13}C > +0.37\,(2\sigma)$. We use the abundance pattern of this DLA, combined with a stochastic chemical enrichment model, to infer the properties of the enriching stars, finding the total gas mass of this system to be $\log_{10}(M_{\rm gas}/{\rm M}_\odot) = 6.3^{+1.4}_{-0.9}$ and the total stellar mass to be $\log_{10}(M_\star/{\rm M}_\odot) = 4.8 \pm 1.3$. The current observations disfavour enrichment by metal-poor asymptotic giant branch (AGB) stars with masses $< 2.4\,{\rm M}_\odot$, limiting the epoch at which this DLA formed most of its enriching stars. Our modelling suggests that this DLA formed very few stars until $\gtrsim 1$ Gyr after the cosmic reionization of hydrogen and, despite its very low metallicity ($\sim 1/1000$ of solar), this DLA appears to have formed most of its stars in the past few hundred Myr. Combining the inferred star formation history with evidence that some of the *most* metal-poor DLAs display an elevated [C/O] ratio at redshift $z \lesssim 3$, we suggest that very metal-poor DLAs may have been affected by reionization quenching. Finally, given the simplicity and quiescence of the absorption features associated with the DLA studied here, we use these ESPRESSO data to place a bound on the possible variability of the fine-structure constant, $\Delta\alpha/\alpha = (-1.2 \pm 1.1) \times 10^{-5}$.

Key words: stars: Population III – ISM: abundances – quasars: absorption lines – dark ages, reionization, first stars.

1 INTRODUCTION

The earliest episodes of star formation can be studied by measuring the chemical composition of near-pristine environments. Indeed, there may be some environments in the Universe that have been solely enriched by the first generation of metal-free stars (also known as Population III stars) – a population of stars that we still know very little about; we are yet to discover a star that shows no detectable metals. However, dedicated surveys (e.g. Bond 1980; Beers, Preston & Shectman 1985, 1992; Keller et al. 2007; Christlieb et al. 2008; Aoki et al. 2013; Caffau et al. 2013; Li et al. 2015; Aguado et al. 2016; Howes et al. 2016; Starkenburg et al. 2017; Da Costa et al. 2019) have revealed an interesting trend in the chemical composition of the lowest metallicity stars. Notably, there is an overabundance of carbon in some of the most iron-poor stars found in the halo of the Milky Way; indeed, every star with a measured iron abundance [Fe/H] ≤ -5.0 exhibits a strong carbon enhancement[1] (Christlieb et al. 2004; Frebel et al. 2005; Aoki et al. 2006; Allende Prieto et al. 2015; Frebel et al. 2015; Nordlander et al. 2019).

Despite concentrated efforts, and increasingly sophisticated cosmological hydrodynamic simulations, we have yet to establish whether or not low-mass ($\sim 1\,{\rm M}_\odot$) metal-free stars can form. Seminal simulations of Population III star formation, like those of Tegmark et al. (1997), Barkana & Loeb (2001), Abel, Bryan & Norman (2002), and Bromm, Coppi & Larson (2002), suggested an initial mass range from $100 - 1000\,{\rm M}_\odot$. As the resolution of these simulations improved, alongside our ability to incorporate more detailed physics, the predicted minimum mass of the first stars has decreased. Current simulations suggest that Population III stars were dominated by stars in the mass range $10 - 100\,{\rm M}_\odot$ (Turk, Abel & O'Shea 2009; Greif et al. 2010; Clark et al. 2011; Hirano et al. 2014; Stacy, Bromm & Lee 2016). Given that we

[1] Here, and throughout this paper, [X/Y] denotes the logarithmic number abundance ratio of elements X and Y relative to their solar values $X_\odot$ and $Y_\odot$, i.e. $[X/Y] = \log_{10}(N_X/N_Y) - \log_{10}(N_X/N_Y)_\odot$.

★ E-mail: louise.a.welsh@durham.ac.uk

are yet to discover a metal-free star around the Milky Way, one might conclude that Population III stars were dominated by more massive ($> 10 M_\odot$) stars that lived relatively short lives. There are, however, simulations that suggest low-mass Population III stars can form, either through efficient fragmentation of the primordial gas (Clark et al. 2011; Stacy et al. 2016) or through the re-cooling of preserved pristine gas that has been photoionized by a nearby burst of metal-free star formation (Stacy & Bromm 2014).

A complementary approach to study the imprints of Population III stars in second generation (Population II) stars is the analysis of metal-poor absorption line systems (Erni et al. 2006; Pettini et al. 2008; Penprase et al. 2010). Of all known damped Ly α systems (DLAs, which are defined as absorption line systems with a neutral hydrogen column density $\log_{10} N(\mathrm{H\,I})/\mathrm{cm}^{-2} > 20.3$), only one gas cloud reportedly shows a carbon enhancement similar to that seen in metal-poor halo stars (Cooke et al. 2011a; see also, Dutta et al. 2014; Cooke, Pettini & Jorgenson 2015). This system is located at a redshift $z_{\rm abs} \simeq 2.34$ along the line of sight to the quasar SDSS J003501.88–091817.6 (hereafter J0035–0918), and displays a large column density of neutral hydrogen, $\log_{10} N(\mathrm{H\,I})/\mathrm{cm}^{-2} = 20.43 \pm 0.04$. Previous observations of this DLA towards J0035–0918 have shown that it is one of the least polluted reservoirs of neutral gas currently known, with a relative iron abundance almost 1/1000 that of the Sun. DLAs are thought to be self-shielded from external radiation due to their large H I column density; their constituent elements tend to exist in a single, dominant ionization state. We can therefore determine the chemical abundance patterns of these systems without needing to apply ionization corrections. We note there are some reservoirs of partially ionized gas that show *no* detectable metals (e.g. Fumagalli, O'Meara & Prochaska 2011 and Robert et al. 2019). The metal paucity of the DLA towards J0035–0918, alongside the originally reported overabundance of carbon, makes this an interesting environment to search for signatures of Population III stars.

Here, we propose an observational approach to assess the existence or absence of low-mass Population III stars. Simulations of stellar evolution have shown that most stellar populations predominantly produce ^{12}C. There are only two channels through which low values of $^{12}\mathrm{C}/^{13}\mathrm{C}$ can be produced. These involve either: (1) low-mass metal-free stars; or (2) metal-poor intermediate mass asymptotic giant branch (AGB) stars (Campbell & Lattanzio 2008; Karakas 2010). Note that both metal-free and metal-enriched massive stars (i.e. $M > 10\,\mathrm{M}_\odot$) produce $^{12}\mathrm{C}/^{13}\mathrm{C} > 100$ (Heger & Woosley 2010).[2] Therefore, by measuring the carbon isotope ratio of a near-pristine gas cloud, we can test if low-mass Population III stars might have contributed to the enrichment. Moreover, because stars of different mass produce different quantities of $^{12}\mathrm{C}/^{13}\mathrm{C}$, we can use the measured abundance as a 'clock' to infer the enrichment time-scale of a system. As only the intermediate mass metal-poor stars produce significant yields of ^{13}C, there is a finite time in which a system will retain a distinctive low $^{12}\mathrm{C}/^{13}\mathrm{C}$ signature before the ^{12}C-rich yields of low-mass stars return the isotope ratio to larger values.

A measurement of the carbon isotope ratio in near-pristine gas relies on our ability to distinguish absorption lines that are separated by a small isotope shift; for the C II λ1334 absorption line, ^{13}C is shifted by -2.99 km s^{-1} relative to ^{12}C. In typical metal-poor DLAs, the overall line profile contains a small number ($\lesssim 5$) of absorption clouds spread over a velocity interval of tens km s^{-1}, where each individual absorption component exhibits a total line broadening of 3 – 5km s^{-1}. The DLA towards J0035–0918 is particularly quiescent, where the absorption is concentrated in a single component with an estimated total Doppler width of $b \simeq 3.5$ km s^{-1}(Cooke et al. 2015), which is related to the velocity dispersion of the gas, $\sigma = \sqrt{2}\,b$. With such a system, it may be possible to detect ^{13}C as an asymmetry of the C II λ1334 feature. Such an asymmetry will not be present in the absorption lines of other elements.

A measurement of the $^{12}\mathrm{C}/^{13}\mathrm{C}$ ratio has never been attempted in a near-pristine environment. The only high redshift bound currently available using absorption line techniques was based on neutral C I absorption lines associated with a metal-rich ([Zn/H] $= -0.49$) sub-DLA towards HE 0515–4414 (Levshakov et al. 2006). This study utilized the Ultraviolet and Visual Echelle Spectrograph (UVES; Dekker et al. 2000) at the European Southern Observatory (ESO) Very Large Telescope (VLT), and reported a limit $^{12}\mathrm{C}/^{13}\mathrm{C} > 80$ (95 per cent confidence).

Complementary high-redshift measurements of the $^{12}\mathrm{C}/^{13}\mathrm{C}$ isotope ratio are afforded by sub-mm studies of the ^{12}CO and ^{13}CO emission lines (Béthermin et al. 2018). However, the sensitivity of current instrumentation means that these works are generally focused on relatively metal-rich galaxies at high redshift.

To reach the required level of accuracy, we need to employ a very high spectral resolution instrument that has an accurate wavelength calibration. Such a requirement is now met with the Echelle SPectrograph for Rocky Exoplanet and Stable Spectroscopic Observations (ESPRESSO; Pepe et al. 2010) at the ESO VLT. This high resolution ($R \simeq 70\,000 - 140\,000$) spectrograph provides an unprecedented level of wavelength accuracy; when used in 4UT mode, the relative velocity accuracy is better than 5 m s^{-1}, corresponding to an accuracy of $\sim 10^{-4}$ Å at 4000 Å.

In this paper, we present the first bound on the $^{12}\mathrm{C}/^{13}\mathrm{C}$ isotope ratio of the DLA towards J0035–0918 using ESPRESSO data obtained during the science verification process. These data have also allowed us to explore the chemical enrichment history of this DLA and to place a bound on the fine-structure constant variation. The paper is organized as follows. Section 2 describes our observations and data reduction. In Section 3, we present our data and determine the chemical composition of the DLA towards J0035–0918 using the detected metal absorption line profiles. We then discuss the chemical enrichment history of this system and infer some of its physical properties in Section 4, before drawing overall conclusions and suggesting future work in Section 5.

2 OBSERVATIONS AND DATA REDUCTION

J0035–0918 is a $m_r = 18.89$ quasar at $z_{\rm em} = 2.42$ whose line of sight intersects a large pocket of neutral hydrogen. This intervening gas cloud was identified as a DLA at $z_{\rm abs} \simeq 2.34$ from the Sloan Digital Sky Survey (SDSS) discovery spectrum. The lack of metal lines associated with this DLA motivated follow up observations with the HIgh Resolution Echelle Spectrograph (HIRES; Vogt et al. 1994) on the Keck I telescope by Cooke et al. (2011a). Further observations were carried out using UVES by Dutta et al. (2014). The combined analysis of these UVES and HIRES data revealed that the DLA towards J0035–0918 is one of the least polluted neutral gas clouds currently known with [Fe/H] $= -2.94 \pm 0.06$ (Cooke et al. 2015). Furthermore, it is the only very metal-poor DLA to show an overabundance of carbon relative to iron, [C/Fe] $= +0.58 \pm 0.16$ (Cooke et al. 2015). An enhancement of carbon is thought to be

[2]While we utilize the yields of non-rotating stellar models, we note that extremely metal-poor, rapidly rotating massive ($> 7\mathrm{M}_\odot$) stars are capable of producing $4 < {}^{12}\mathrm{C}/^{13}\mathrm{C} < 77$ (Meynet et al. 2010).

a chemical signature of Population III enriched systems (Beers & Christlieb 2005). While the DLA towards J0035–0918 is not carbon enhanced to the same degree exhibited by some metal-poor stars, its enhancement of C and N relative to Fe is a rarity amongst the very metal-poor DLA population.

Previous observations indicated that the DLA towards J0035–0918 is particularly quiescent, with a single absorption component exhibiting a total Doppler parameter of $b \simeq 3.5\,\mathrm{km\,s^{-1}}$(Cooke et al. 2015). The ^{12}C and ^{13}C isotopes produce rest-frame absorption features at λ1334.5323 Å and λ1334.519 Å, respectively (Morton 2003); the isotope shift is therefore just 2.99 km s^{-1}. Given the narrow broadening of this system, it is therefore possible to distinguish between the contribution of each C isotope to the total C II λ1334 line profile. Thus, the DLA towards J0035–0918 is a near-ideal environment to measure the carbon isotope ratio and search for the chemical signature of low-mass ($\sim 1\,\mathrm{M_\odot}$) Population III stars. Given the potential promise of this system, we secured new observations with the ultrastable ESO ESPRESSO spectrograph.

New data were collected with ESPRESSO in 4UT mode ($R \simeq 70\,000$) on 2019 August 28 spanning the wavelength range 3800 – 7880 Å. We acquired 3 × 2100 s exposures on target using 8 × 4 binning in slow readout mode. In 4UT mode, the light from the four UTs is incoherently sent to ESPRESSO. The size of the entrance fibre at each UT is 1.0 arcsec. The average seeing during our observations was 0.64 arcsec. These data were reduced using the EsoRex pipeline, including the standard reduction steps of subtracting the detector bias, locating and tracing the echelle orders, flat-fielding, extracting the 1D spectrum, performing a wavelength calibration, and relative flux calibrations.

Due to the faint nature of our target, we have not performed the conventional sky subtraction which would introduce additional sky and read noise into our data.[3] Given that we are already nearing the magnitude limit of what is feasible with this instrument, we decided to maximize the final combined signal-to-noise ratio (S/N) and model the zero level of the data in our analysis. This will be discussed further in Section 3.

As a final step, we combined the three individual exposures using UVES_POPLER[4] with a pixel sampling of 2 km s^{-1}. UVES_POPLER allowed us to manually mask cosmic rays and minor defects from the combined spectrum. The final combined S/N of the data near the C II λ1334 absorption line (at observed wavelength $\lambda_{\rm obs} = 4457.8$ Å) is S/N ≃ 9. The peak S/N of the data is near 5300 Å (S/N ≃ 30). As will be described in the following section, alongside these ESPRESSO data, we utilize the spectra from previous observations of the DLA towards J0035–0918 to model the metal line profiles of this absorption system. These data were recorded with a resolution of $R \simeq 40\,000$ and a reported S/N per pixel of S/N ≃ 18 at 4500 Å (Cooke et al. 2011a) and S/N ≃ 13 at 5000 Å (Dutta et al. 2014). We refer the reader to these publications for details of these data.

3 RESULTS

We exploit the superior wavelength calibration of ESPRESSO to pin down the redshift of the DLA using O, Al, Si, and Fe absorption lines, and search for a shift/asymmetry of the C II line profile – *relative* to the other metals – indicative of absorption from ^{13}C.

Using the Absorption LIne Software (ALIS) package[5] – which employs a χ-squared minimization procedure to find the model parameters that best describe the input data – we simultaneously analyse the full complement of high S/N and high spectral resolution data currently available. While the ESPRESSO data provide the most reliable wavelength solution, the UVES and HIRES data can be leveraged alongside the ESPRESSO data to enable a more accurate determination of the metal ion column densities and assist in the determination of the zero-level of the ESPRESSO data. To achieve this, the redshift of the DLA is driven by the accurate wavelength solution provided by the ESPRESSO data. The centre of each absorption feature in the UVES and HIRES data is then modelled with an independent velocity offset to ensure that these data are coincident with the well-calibrated ESPRESSO data.

We model the absorption line profiles as a single-component Voigt profile, which consists of three parameters: a column density, a redshift, and a line broadening. We assume that all lines of comparable ionization level have the same redshift, and any absorption lines that are produced by the same ion all have the same column density. The total broadening of the lines includes a contribution from both turbulent and thermal broadening. The turbulent broadening is assumed to be the same for all absorption features, while the thermal broadening depends inversely on the square root of the ion mass; thus, heavy elements (e.g. Fe) will exhibit absorption profiles that are intrinsically narrower than the profiles of lighter elements, (e.g. C). There is an additional contribution to the line broadening due to the instrument.

The nominal ESPRESSO instrument resolution in 4UT mode is $v_{\rm FWHM} = 4.28$ km s^{-1}, and we have explicitly checked this by measuring the widths of ThAr emission lines from the calibration data to infer the instrument full width at half maximum (FWHM) at wavelengths close to the DLA's absorption features. We find that across the wavelength range (4450 – 7830)Å the wavelength specific FWHM varies from 4.14 to 4.53 km s^{-1}. We adopt these wavelength specific resolutions as our fiducial choice when fitting the data. However, we also checked that our results did not change when using the nominal instrument FWHM. For the HIRES and UVES data, the respective nominal instrument resolutions are $v_{\rm FWHM} = 8.1$ km s^{-1} and $v_{\rm FWHM} = 7.75$ km s^{-1}. When fitting to the data, we allow these to vary as free parameters, since the DLA absorption features are unresolved in the UVES and HIRES data. We found that the choice of instrument resolution does not have a significant impact on the resulting column densities. We have performed additional checks to ensure that the system is best modelled by a single absorption component with a stable redshift; for example, we included fictitious isotope transitions in the fit to the line profiles of other elements (like Si II), and these tests demonstrated that the absorption profiles preferred a single, symmetric absorption line. We have also tested that our result cannot be replicated using a 'mirrored' ^{13}C feature that has an offset from ^{12}C of +2.99 km s^{-1} (instead of the true value, −2.99 km s^{-1}).

Finally, we note that we simultaneously fit the absorption, quasar continuum, and in the case of the ESPRESSO data, the zero-level of the data. We model the continuum around every absorption line as a low order Legendre polynomial (of order 3). We assume that the zero-levels of the sky-subtracted UVES and HIRES data do not depart from zero (this is confirmed by measuring the troughs of

[3]This is because the science and sky fibres project to the same number of pixels on the detector. For faint objects, performing a sky subtraction results in counting the sky and read noise twice.

[4]UVES_POPLER is available from: https://astronomy.swin.edu.au/~mmurphy/UVES_popler/

[5]ALIS is available from: https://github.com/rcooke-ast/ALIS.

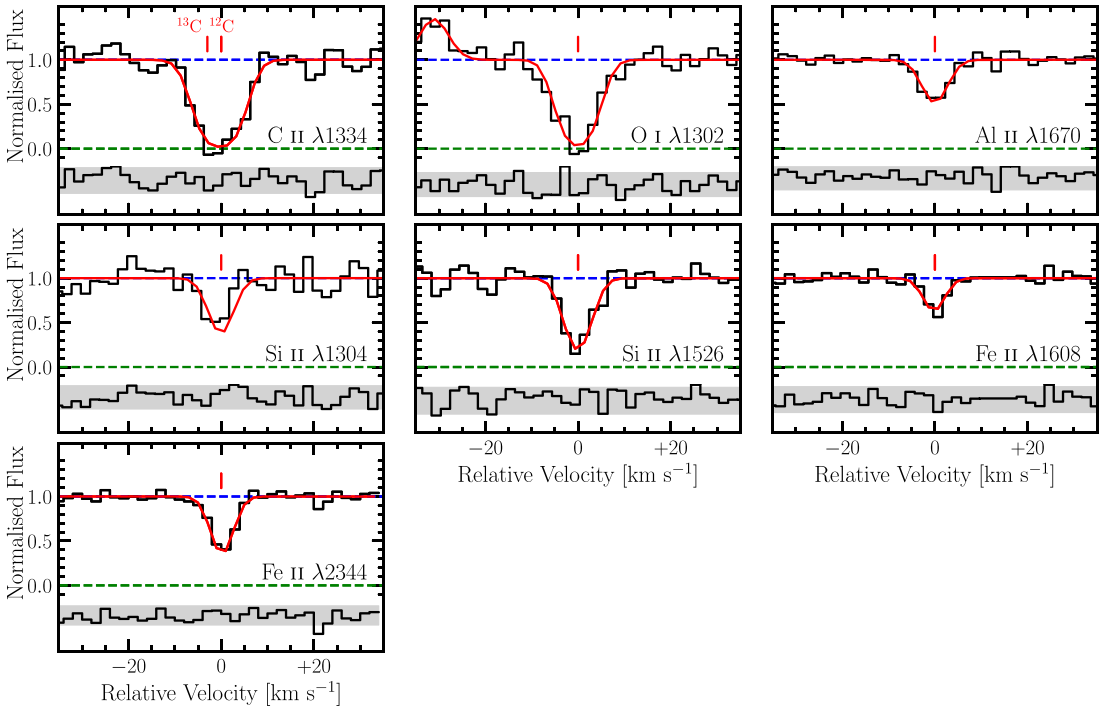

Figure 1. Continuum normalized ESPRESSO data (black histograms) of the absorption features produced by metal ions associated with the DLA at $z_{\rm abs} = 2.340\,064$ towards the quasar J0035–0918. Overplotted in red is our best-fitting model. The blue dashed line indicates the position of the continuum while the green dashed line indicates the zero-level. The red ticks above the absorption features indicate the centre of the Voigt line profiles. In the panel that shows C II λ1334 absorption, the tick marks at a relative velocity of 0.0 and −2.99 km s^{-1} represent the centroid of the ^{12}C and ^{13}C absorption line profiles, respectively. Below the zero-level, we show the residuals of this fit (black histogram) where the grey shaded band encompasses the 2σ deviates between the model and the data. Note, in the panel corresponding to O I λ1302, there is an unrelated emission line (due to an unrelated, intervening galaxy at redshift $z \simeq 0.15$; see text) that we have modelled as a Gaussian during the line-fitting procedure.

Table 1. Ion column densities of the DLA at $z_{\rm abs} = 2.340\,064$ towards the quasar J0035–0918. The quoted column densities are based on the combined fit of the available ESPRESSO, UVES, and HIRES data. The quoted column density errors are the 1σ confidence limits. We also report the carbon isotope ratio as a 2σ limit.

Ion	$\log_{10} N$(X)/cm^{-2}
H I	20.43 ± 0.04[a]
^{12}C II + ^{13}C II	14.29 ± 0.13
N I	13.37 ± 0.04
O I	14.67 ± 0.05
Mg II	12.89 ± 0.13
Al II	11.74 ± 0.04
Si II	13.35 ± 0.04
Fe II	13.01 ± 0.03
Isotope ratio	
$\log_{10} N(^{12}{\rm C})/N(^{13}{\rm C}) > +0.37\ (2\sigma)$	

[a]The H I column density was reported by Cooke et al. (2015).

saturated absorption lines). Upon inspection of the sky-subtracted ESPRESSO data, we identified a few emission lines that appear to be due to contamination by a nearby galaxy in the field. These emission lines are not present in the UVES or HIRES data. The redshift of this galaxy was determined through observations using the William Herschel Telescope (WHT) that revealed strong O II λ3727 Å emission at an observed wavelength $\lambda \simeq 4297$ Å, corresponding to $z \simeq 0.15$. This galaxy is just 6.8 arcsec from the line of sight to the background quasar (corresponding to an impact parameter of 21 kpc at the redshift of the intervening galaxy). We confirmed that there are no sky or galaxy emission lines that contaminate the DLA absorption lines. Therefore to account for the sky continuum and potential low-level contamination by the continuum of this low-redshift galaxy, we include a single parameter to model the zero-level of the ESPRESSO data (assumed constant for all lines).

3.1 Ion column densities

The ESPRESSO data, along with the best-fitting model are presented in Fig. 1, while the corresponding column densities are listed in Table 1.

The simultaneous analysis of the ESPRESSO+HIRES+UVES data have allowed us to accurately determine the metal column densities, gas kinetic temperature, and total Doppler parameter of the DLA. We find an absorption redshift of $z_{\rm abs} = 2.340\,064 \pm 0.000\,001$ and a gas temperature of $T = (9.1 \pm 0.5) \times 10^3$ K. We have found that the line broadening of this system is entirely dominated by its thermal motions; the minor contribution due to the turbulent motions cannot be determined given the current data and, intriguingly, is consistent with no turbulence. The extreme quiescence of this system raises an interesting possibility about the existence of other thermally dominated DLAs yet to be found, or whether known systems that contain multiple absorption components, may still have components that are dominated by thermal broadening.

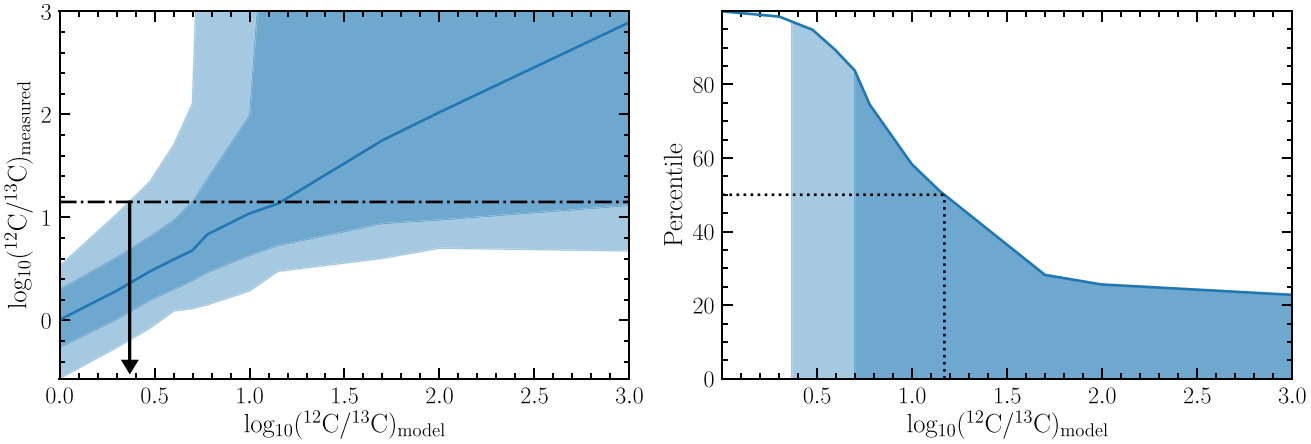

Figure 2. Monte Carlo simulations of our data used to infer a confidence bound on the amount of ^{13}C in the DLA towards J0035–0918 (left-hand panel). The blue line indicates the median recovered value of the $^{12}C/^{13}C$ ratio given 500 realizations of the absorption feature generated using the model $^{12}C/^{13}C$ ratio indicated by the *x*-axis. The dark and light blue shaded bands encompass the 1σ and 2σ limits of the distribution, respectively. The horizontal dot–dashed line marks the $^{12}C/^{13}C$ measured in our analysis. The black arrow indicates where this value intersects the 97.5 percentile of the distribution. This corresponds to a 2σ lower limit of $^{12}C/^{13}C > +0.37$. The right-hand panel shows the percentile value as a function of the model (i.e. true) $^{12}C/^{13}C$ isotope ratio given our measured value. The shaded bands have the same meaning as in the left-hand panel. The dotted lines mark the 50th percentile and the corresponding model value.

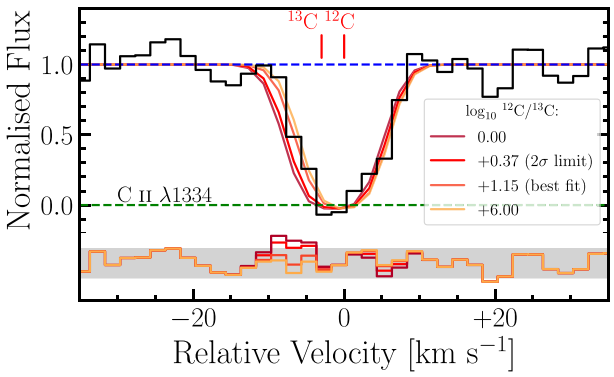

Figure 3. ESPRESSO data centred on the C II λ1334 absorption feature shown alongside different model line profiles. Each model curve represents a different $^{12}C/^{13}C$ abundance ratio (as indicated by the legend) while retaining a constant total carbon abundance of $\log_{10} N(C_{tot})/cm^{-2} = 14.29$. Below the zero-level of these data (green dashed line), we show the residuals of the model fit to the data. The shaded band encompasses the 2σ deviations of these model profiles, illustrating that we can rule out $\log_{10}{}^{12}C/^{13}C \leq +0.37$ with 95 per cent confidence.

For the C II absorption, we found that the best-determined parameter combination was the isotope ratio $^{12}C/^{13}C$ and the total column density of C II, $N(^{12}C\,II) + N(^{13}C\,II)$. The carbon isotope ratio of this model is $\log_{10}{}^{12}C/^{13}C = +1.15 \pm 0.65$, where the quoted error is simply the diagonal term of the covariance matrix. However, given the large range allowed by this uncertainty, we have performed a suite of detailed Monte Carlo simulations to uncover the posterior distribution of the $^{12}C/^{13}C$ ratio, given our data. Using the parameters of our best-fitting line model, we generate mock ESPRESSO data varying the relative amount of ^{13}C in the system. These mock data provide perfect (error free) line profiles of C II λ1334 for different values of the $^{12}C/^{13}C$ isotope ratio (while the total C II column density remains constant). By perturbing these line profiles using the error spectrum of our data, we can emulate how these ESPRESSO data would look as a function of the underlying isotope ratio. We have performed 500 realizations of these perturbations for a variety of underlying isotope ratios. The results of these simulations are presented in Fig. 2. Given that our line fitting procedure, applied to the real data, suggests a central value $\log_{10}{}^{12}C/^{13}C = +1.15$, we infer $\log_{10}{}^{12}C/^{13}C > +0.37$ (2σ). This lower bound is visualized in Fig. 3, which shows the model line profiles for various $^{12}C/^{13}C$ abundance ratios. The line corresponding to $\log_{10}{}^{12}C/^{13}C = +0.37$ falls at the edge of the asymmetric line profile where the ^{13}C absorption is most noticeable; the corresponding residuals are also at the 2σ boundary of the model fit. As the amount of ^{12}C relative to ^{13}C in a system increases, the asymmetry due to the presence of ^{13}C becomes increasingly subtle in the C II λ1334 line profile. This is, in part, why we expect to recover a broad range of isotope ratios once $\log_{10}{}^{12}C/^{13}C > +1.10$. However, we expect with higher S/N data, the threshold for a detection would extend to larger isotope ratios.

Table 2. Relative abundances of the elements detected in the DLA towards J0035–0918 alongside their solar abundances as determined by Asplund et al. (2009).

X	[X/H]	[X/Fe]	[X/O]	$X_\odot$
C	-2.57 ± 0.14	$+0.32 \pm 0.13$	-0.12 ± 0.14	8.43
N	-2.89 ± 0.06	0.00 ± 0.05	-0.44 ± 0.06	7.83
O	-2.45 ± 0.06	$+0.44 \pm 0.06$	–	8.69
Mg	-3.10 ± 0.14	-0.21 ± 0.13	-0.65 ± 0.14	7.56
Al	-3.13 ± 0.06	-0.24 ± 0.05	-0.68 ± 0.06	6.44
Si	-2.59 ± 0.06	$+0.30 \pm 0.05$	-0.14 ± 0.06	7.51
Fe	-2.89 ± 0.05	–	-0.44 ± 0.06	7.47

This is the first limit on the carbon isotope ratio in a near-pristine absorption system. With these data we can empirically rule out the presence of large amounts of ^{13}C relative to ^{12}C in the DLA towards J0035–0918. The implications of this abundance ratio for the chemical enrichment of this DLA will be discussed in Section 4. The relative abundances of the detected metals are provided for convenience in Table 2. We note that with the latest data, [C/Fe] $= +0.32 \pm 0.13$. While consistent with the previous determinations by Carswell et al. (2012), Dutta et al. (2014),

and Cooke et al. (2015), this indicates that the DLA towards J0035–0918 is not as abundant in carbon as previously thought, owing to the unusual quiescence of the gas cloud whose broadening is dominated by the thermal motions. However, this system still exhibits an unusually high [N/O] ratio, compared with the typical very metal-poor DLA population (Cooke et al. 2011b). The [N/O] abundance of this DLA places it just above the primary N plateau (Petitjean, Ledoux & Srianand 2008; Pettini et al. 2008; Zafar et al. 2014). Furthermore, the [Mg/Si], [Mg/O], and [Mg/Fe] ratios are remarkably subsolar, quite unlike the ratios that are seen in extremely metal-poor halo stars of the Milky Way (e.g. Andrievsky et al. 2010).

4 ANALYSIS

Given our robust determination of the chemical abundance pattern of the DLA towards J0035–0918, we now investigate the enrichment history of this system. Our lower bound on the $^{12}C/^{13}C$ isotope ratio indicates that there is at least 2.3 times more ^{12}C than ^{13}C in this DLA; this does not empirically rule out enrichment from low-mass Population III stars. To test whether the chemical signature of this system is better modelled by Population III or Population II enrichment, we can exploit the stochastic chemical enrichment model developed by Welsh, Cooke & Fumagalli (2019), alongside the yields from simulations of stellar evolution. The resulting enrichment models can be used to infer the epoch at which this DLA formed its enriching stars as well as its total stellar mass and total gas mass. In addition to investigating the physical and chemical properties of the DLA towards J0035–0918, given the simplicity of the absorption line profiles and the reliable wavelength solution delivered by ESPRESSO, we can also use these data to test the invariance of the fine-structure constant.

4.1 Stochastic enrichment model

In previous work (Welsh et al. 2019), we developed a stochastic chemical enrichment model that uses the abundance patterns of near-pristine environments to infer their chemical enrichment history. This model describes the initial mass function (IMF) of an enriching stellar population as a power law, governed by the slope, α. The normalization of this power law, k, is set by the number of stars, $N_\star$, that form within a given mass range:

$$N_\star = \int_{M_{\rm min}}^{M_{\rm max}} kM^{-\alpha}{\rm d}M. \quad (1)$$

For reference, a Salpeter IMF corresponds to $\alpha = 2.35$ (Salpeter 1955). For a given enrichment model, we then stochastically sample the IMF and, using the yields from simulations of stellar evolution, determine the distribution of chemical abundances we expect to see across an enriched population of objects. These distributions can then be used to gauge the likelihood of measuring our observed abundances given any underlying enrichment model. This approach assumes that the gas within the DLA is well-mixed and that the system experiences no inflow or outflow of gas; for further details of this model, see Welsh et al. (2019).

The stellar yields used in this analysis are from three sources: (1) Campbell & Lattanzio (2008), hereafter CL08, who simulate the evolution of low-mass metal-free stars in the mass range $(1-3)\,M_\odot$; (2) Karakas (2010), hereafter K10, who simulate the evolution of very metal-poor AGB stars ($Z \sim 0.005\,Z_\odot$) in the mass range $(1-6)\,M_\odot$; and, (3) Heger & Woosley (2010), hereafter HW10, who simulate the evolution and core-collapse supernovae (CCSNe) of massive ($> 10M_\odot$) metal-free stars. Throughout this work, we use the combined yields of CL08 and HW10 to define the yields of Population III stars. In lieu of simulations that calculate the $^{12}C/^{13}C$ yield of intermediate mass Population III stars, we have chosen to extrapolate the yields of CL08 to meet the yields of HW10.

While the HW10 yields have been calculated for metal-free stars, they are also indicative of Population II CCSNe yields; this can be seen by comparison with the Woosley & Weaver (1995) yields of metal-enriched massive stars (at least for the elements under consideration in this work). We therefore define Population II yields as the combined yields of K10 and HW10. We necessarily implement another yield extrapolation to bridge the gap between the K10 and HW10 yields. Although this extrapolation is not ideal, this is the best option available to us until a more complete set of yields becomes available. K10 report stellar yields covering a range of metallicities, spanning $0.0001 < Z < 0.02$. We choose Population II yields with an initial metallicity $Z = 0.0001$. We note that the HW10 yields have been calculated as a function of the progenitor star mass, the explosion energy of their supernova, and the mixing between the different stellar layers. When considering these yields, we have adopted the recommended prescription for mixing between stellar layers, defined to be 10 per cent of the helium core size. For the explosion energy, we adopt $E_{\rm exp} = 1.8 \times 10^{51}$ erg. This is a measure of the final kinetic energy of the ejecta at infinity and is consistent with the typical value found by Welsh et al. (2019) when investigating the properties of the stars that enrich the most metal-poor DLAs. Fig. 4 shows the resulting $^{12}C/^{13}C$ yields of these stellar populations as a function of both their progenitor mass and stellar lifetime.

From Fig. 4, we can see that it is the low-mass Population III stars, and the intermediate mass Population II stars, that are capable of producing comparable amounts of the carbon isotopes (i.e. $^{12}C/^{13}C \simeq 1$). Generally, it is surface mixing events that facilitate the production of ^{13}C. AGB (both Population II and Population III) stars produce ^{13}C through a process known as hot bottom burning (HBB). This process involves the convection induced transport of ^{12}C from the burning shell to the proton-rich envelope where ^{13}C can then be synthesized via proton-capture (Iben 1975; Prantzos, Aubert & Audouze 1996). HBB is dependent on both the mass and metallicity of the progenitor stars. For a star to undergo HBB, the convective envelope must reach a sufficiently high temperature. The transition seen at $\sim 10\,M_\odot$ between the yields of massive stars and those of lower mass stars originates because massive stars do not show signs of these surface mixing events (Karakas & Lattanzio 2014); they are only capable of producing ^{13}C through secondary processes.

Using our enrichment model with the above yields, we can investigate the chemical enrichment of the DLA towards J0035–0918 under the assumption of either Population II or Population III enrichment. We use the relative abundances of [C/O], [Si/O], and [Fe/O] as given in Table 2, alongside the lower limit on $^{12}C/^{13}C$ listed in Table 1 to evaluate the likelihood of a given model. We choose to model only these abundance ratios because our stochastic chemical enrichment model is computationally expensive. We therefore focus our attention on the most abundant elements that are relatively well-modelled by stellar evolution. We use the EMCEE Markov Chain Monte Carlo (MCMC) sampler (Foreman-Mackey et al. 2013) to determine the enrichment model parameters that provide the best fit to these data. The model parameters that we consider are those defined by equation (1) (α, $N_\star$, $M_{\rm min}$, $M_{\rm max}$). We

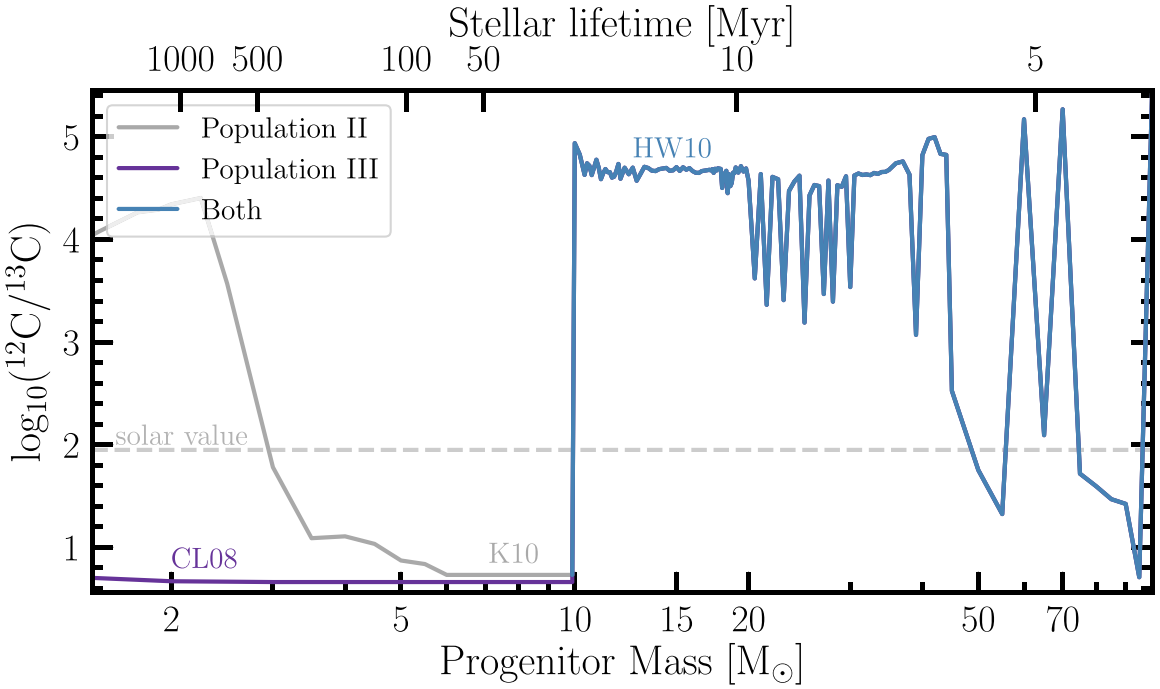

Figure 4. $^{12}C/^{13}C$ yields as a function of progenitor mass for both Population III and Population II stars. The yields of low-mass Population III stars are from CL08 while those of Population II stars are from K10. The yields of massive Population III and Population II stars are given by HW10. We have only included the yields of stars whose lifetimes are shorter than the age of the Universe at $z = 2.34$ (i.e. those with $M > 1.46\ M_\odot$). The stellar lifetimes are indicated by the top x-axis (Woosley, Heger & Weaver 2002, Karakas 2014). The horizontal grey dashed line indicates the solar C isotope ratio, $^{12}C/^{13}C = 89$ (Asplund et al. 2009).

impose uniform priors on these parameters, limited by the boundary conditions

$$\begin{aligned} 0 \leq &\quad \log_{10} N_\star &&\leq 5, \\ 1.46 \leq &\quad M_{\rm min}/M_\odot &&\leq 11, \\ 20 \leq &\quad M_{\rm max}/M_\odot &&\leq 70, \\ -8 \leq &\quad \alpha &&\leq 8\,. \end{aligned}$$

Since the *number* of stars contributing to the enrichment of the DLA, $N_\star$, could be quite large in the case of a low value of $M_{\rm min}$, we choose to sample $\log_{10} N_\star$; this allows us to stochastically sample the IMF at high masses (a regime we suspect may be dominated by just a few massive stars), while still allowing for a much larger number of low-mass stars. The minimum mass of the enriching stars is set by considering the age of the Universe at the redshift of the DLA. Using the latest Planck Collaboration VI (2018) cosmology, where $H_0 = 67.4 \pm 0.5$ km s^{-1}Mpc^{-1} and $\Omega_{\rm m} = 0.315 \pm 0.007$, we find that the age of the Universe is 2.792 Gyr at the redshift of this absorption system (recall $z_{\rm abs} = 2.34$). Given that the first stars are thought to have formed between $z \sim 15 - 20$, there is a finite time in which stars can contribute to the enrichment of this system. Using the stellar lifetimes from Karakas (2014), we find that stars with masses $\lesssim 1.46\ M_\odot$ live longer than the age of the Universe at redshift $z \simeq 2.34$. Therefore, we only expect to see the chemical signature of stars with masses above this limit in the chemistry of this near-pristine DLA. The upper limit of the mass of the enriching stars marks the transition from CCSNe to pulsational pair instability SNe, as found by Woosley (2017).

During our MCMC analysis, we utilize the chains of 400 randomly initialized walkers to determine the posterior distributions of our enrichment model parameters. After adopting a burn-in that is half the original length of the chains, we find the posterior distributions shown in Fig. 5. We found that these distributions are invariant once the walkers have each taken 2100 steps. From this figure, we see that the maximum likelihood enrichment model parameters are almost unchanged by the assumption of Population II versus Population III enrichment. Both enrichment histories suggest an IMF slope that is preferably steeper than, but still consistent with, a Salpeter distribution, $\alpha = 3.6^{+3.7}_{-2.0}$ (Population II) $\alpha = 3.8^{+3.6}_{-2.0}$ (Population III), where the quoted errors encompass 95 per cent of the parameter distributions. We have repeated our analysis under the assumption of a Salpeter-like IMF slope and found that introducing this prior has a negligible impact on the resulting distributions.

Our analysis suggests that this DLA has been enriched by at least 10 stars, with maximum likelihood values of $\log_{10} N_\star = 2.3^{+2.5}_{-1.4}$ (Population II) and $\log_{10} N_\star = 2.5^{+2.3}_{-1.7}$ (Population III). In each enrichment scenario, $M_{\rm max}$ is unconstrained, with both distributions showing a slight preference towards a larger maximum enriching mass. We find the only parameter estimate that varies significantly between these enrichment histories is that of the minimum enriching mass, $M_{\rm min}$. Under the assumption of Population II enrichment, the data disfavour enrichment from low-mass ($< 2.4\ M_\odot$) stars. While, if this is a Population III enriched system, enrichment from low-mass stars is preferable. This is likely being driven by the divergent yields of [C/O] across the stellar populations. From the simulations of stellar evolution, we see that the lowest mass Population II stars produce supersolar [C/O] relative to our measured value ($[C/O] = -0.12 \pm 0.14$), while the lowest mass Population III stars produce subsolar yields of [C/O]. Given that our maximum likelihood enrichment model is consistent with a well-sampled IMF, to investigate this divergence further, we can calculate the IMF weighted abundance of [C/O] for both Population II and Population III enrichment. These calculations show that, given our maximum

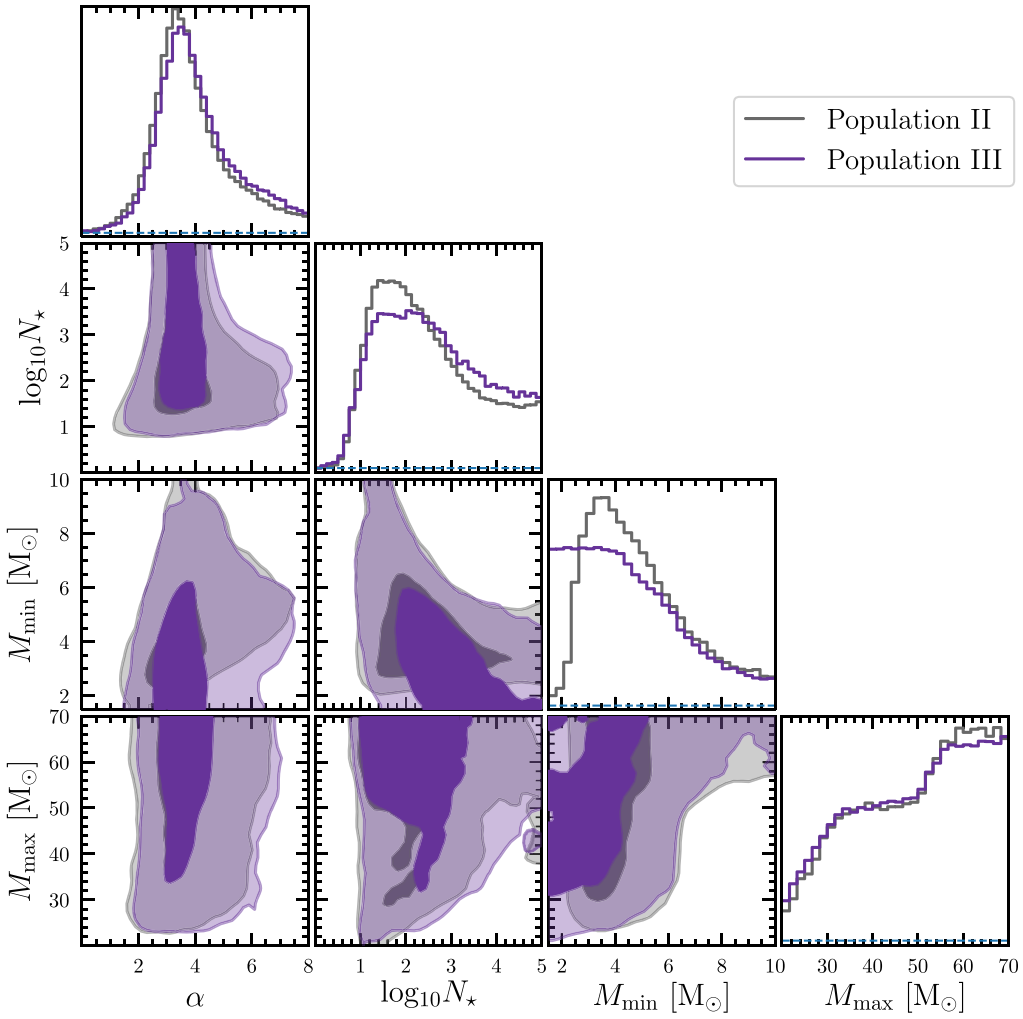

Figure 5. Results of our MCMC analysis of the chemical enrichment of the DLA towards J0035–0918. The diagonal panels indicate the maximum likelihood posterior distributions of our enrichment model parameters while the 2D contours indicate the correlation between these parameters. Our Population II model is shown in grey. Overplotted in purple is the result of considering Population III stars as the dominant source of enrichment. In the diagonal panels, the horizontal blue dashed line indicates the zero-level of each distribution.

likelihood estimate of α, when $M_{\rm min} < 2.4$ M$_\odot$ the C-rich yields of the lowest mass Population II stars result in supersolar [C/O]. These yields are hard to reconcile with our measured value.

Given current data, we are only able to utilize the ^{12}C/^{13}C lower bound to constrain our enrichment model. This lower bound does little to drive the results of our current analysis. However, as can be seen from Fig. 4, the C isotope ratio is also divergent at low masses for the different stellar populations. Therefore, a precise measurement of the ^{12}C/^{13}C ratio, in combination with the [C/O] abundance, would enable us to distinguish more clearly whether the DLA towards J0035–0918 shows the signature of Population III versus Population II enrichment. We also note that there are some extremely metal-poor, rapidly rotating stars, with masses > 7M$_\odot$, that are capable of producing $4 < {}^{12}$C/^{13}C < 77 (Meynet et al. 2010). These stars, that have metallicities between $Z = 5 \times 10^{-7}$ Z$_\odot$ and $Z = 5 \times 10^{-4}$ Z$_\odot$, are capable of producing an enhancement of alpha elements, akin to that observed in the most iron-poor stars of the Milky Way halo. At present, our limit on ^{12}C/^{13}C is not able to rule out rapidly rotating extremely metal-poor stars as a potential source of the enrichment of this near-pristine DLA. However, future higher S/N observations of J0035–0918 will be able to test this possibility.

4.2 Physical and chemical properties

Using the results of our enrichment model analysis, we can infer some of the physical and chemical properties of the DLA towards J0035–0918, such as the total stellar mass and the total gas mass of the system. To calculate the total stellar mass, we use the inferred model parameter distributions and integrate over the IMF, weighted by mass (cf. equation 1). For stars above 1 M$_\odot$, we adopt a power-law IMF, while for stars < 1 M$_\odot$, we adopt the IMF as described by Chabrier (2003). This results in the stellar mass distribution as shown in the left-hand panel of Fig. 6. We find that the total stellar mass (≥ 1 M$_\odot$) of this DLA is $\log_{10}(M_\star/{\rm M}_\odot) = 4.8 \pm 1.3$. We can also infer the total gas mass of the DLA using our enrichment model, as follows. Assuming that the DLA towards J0035–0918 has retained 100 per cent of the metals produced *in situ*, we can calculate the total gas mass required to produce the observed metal abundance. For this calculation, we use the observed [O/H] abundance as a proxy of the metal abundance. The resulting distribution is shown in the right-hand panel of Fig. 6. If this is a Population III enriched system, to achieve the measured abundance [O/H] $= -2.45 \pm 0.06$, we would require a total gas mass $\log_{10}(M_{\rm gas}/{\rm M}_\odot) = 6.3^{+1.4}_{-0.9}$. If, in fact, some metals were not retained

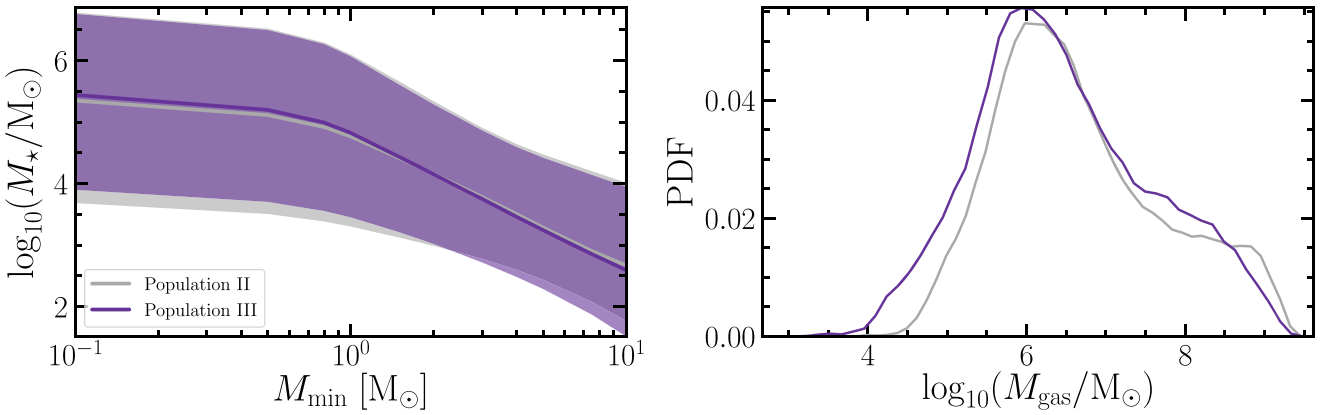

Figure 6. Left: The total inferred stellar mass of the DLA towards J0035–0918 as a function of the minimum mass with which stars can form. The purple solid curve indicates the median value given our Population III enrichment model and the shaded region encompasses the 16th and 84th percentiles. The grey curves have the same meaning, but are based on our Population II enrichment model. Right: The total gas mass of the DLA towards J0035–0918 inferred from our enrichment models combined with the measured [O/H] abundance ([O/H] = −2.45), assuming 100 per cent metal retention (see text for further details).

by the DLA, the observed [O/H] abundance could be achieved through metals mixing with a smaller reservoir of hydrogen. In this case, our inference would correspond to an upper limit of the total gas mass. We find that our inferences of the stellar and gas mass of this DLA are consistent (i.e. within 1σ) of the corresponding values quoted by Welsh et al. (2019) for typical very metal-poor DLAs.

4.3 Enrichment time-scale: Evidence of reionization quenching?

Our constraints on the minimum mass of the enriching stars can be used to estimate the epoch when the DLA experienced most of its star formation. Using the stellar lifetimes from Woosley et al. (2002) and Karakas (2014) as well as the posterior distribution of M_{min} (see the histogram on the third row of Fig. 5), we can convert the M_{min} distribution to a distribution of enrichment time-scales. The results of this transformation for both Population II and Population III stars are shown in Fig. 7. Since our analysis disfavours a large ($\sim 8\,\mathrm{M}_\odot$) minimum enriching mass, the sharp fall of these distributions as we approach the redshift of the DLA suggests that the majority of star formation must have ended prior to this epoch. We can see from this figure that if Population II stars are the predominant enrichers, then the DLA must have had a burst of star formation just a few hundred Myr before we observe the DLA today. Such a time-scale is relatively short given that the DLA would need to have recovered quickly from the putative supernova feedback in order to be observed at $z = 2.34$ with a significant quantity of neutral gas and apparently no turbulence. Hydrodynamic models of the enrichment of ultrafaint dwarf (UFD) galaxies (Webster, Bland-Hawthorn & Sutherland 2015a) indicate that the chemistry of these systems requires periods of extended star formation, which may also be required to explain the enrichment of this DLA (see also, Webster, Bland-Hawthorn & Sutherland 2015b).

In this DLA, however, we find no evidence of enrichment by low-mass Population II stars. As shown in Fig. 7 by the grey curve, the most likely explanation in this scenario is that the DLA experienced no significant star formation post-reionization, for at least $\gtrsim 1$ Gyr. There are several mechanisms that can temporarily quench a low-mass galaxy. One such possibility is reionization quenching (e.g. Bullock, Kravtsov & Weinberg 2000) due to the cosmic reionization of hydrogen at $z \simeq 8$ (Planck Collaboration VI 2018; light blue band in Fig. 7). Reionization played two critical roles that affected star formation in low-mass galaxies. First, reionization heated up the intergalactic medium, thereby limiting the accretion of gas on to low-mass galaxies. This starved low-mass galaxies of the gas supply needed to form stars. Moreover, reionization heated up the interstellar medium of low-mass galaxies, bringing a halt to any ongoing star formation.

The main thrust of current observational efforts to study the reionization quenching of low-mass galaxies utilize deep observations of the lowest mass UFD galaxies orbiting the Milky Way (Weisz et al. 2012; Brown et al. 2014; Weisz et al. 2014). These studies use colour–magnitude diagrams to reconstruct the star formation histories of the UFD galaxies. This technique allows us to study the present properties of UFD galaxies in detail, but currently suffers from poor time resolution at $z \gtrsim 2$. Therefore, it is difficult to study the finer details of the reionization quenching process, such as the duration of the quenching and the properties of the gas that survives reionization. Simulations of low-mass galaxy formation (e.g. Oñorbe et al. 2015; Wheeler et al. 2015) indicate that reionization can bring a halt to star formation for ~ 1 Gyr; furthermore, these simulations indicate that some low-mass galaxies are able to retain a small reservoir of gas for future star formation. Some of these quenched dwarf galaxies may re-ignite their star formation through interactions with gaseous streams in the intergalactic medium (Wright et al. 2019).

Studying the chemical enrichment of the most metal-poor DLAs may therefore offer a novel and exciting opportunity to study reionization quenching in detail by using certain chemical tracers as a 'chemical clock'. Taken at face value, our observations combined with our stochastic chemical enrichment model tentatively suggest that star formation in the DLA towards J0035–0918 may have experienced an ~ 1 Gyr hiatus. In principle, one might be able to tease out the signature of reionization quenching by studying a sample of metal-poor DLAs; reionization is a cosmic event that comparably affects all galaxies at a given mass scale. This signature may be encoded in the star formation histories (and therefore chemistry) of the most metal-poor DLAs. One prediction of this scenario is that the most metal-poor DLAs should exhibit a general increase of their [C/O] at redshift $z \sim 3$; oxygen is primarily produced by massive stars on short time-scales, while carbon is produced by massive stars as well as low- and intermediate-mass stars on longer time-scales (Akerman et al. 2004; Cescutti et al. 2009; Romano et al. 2010). Thus, an increase of [C/O] at low

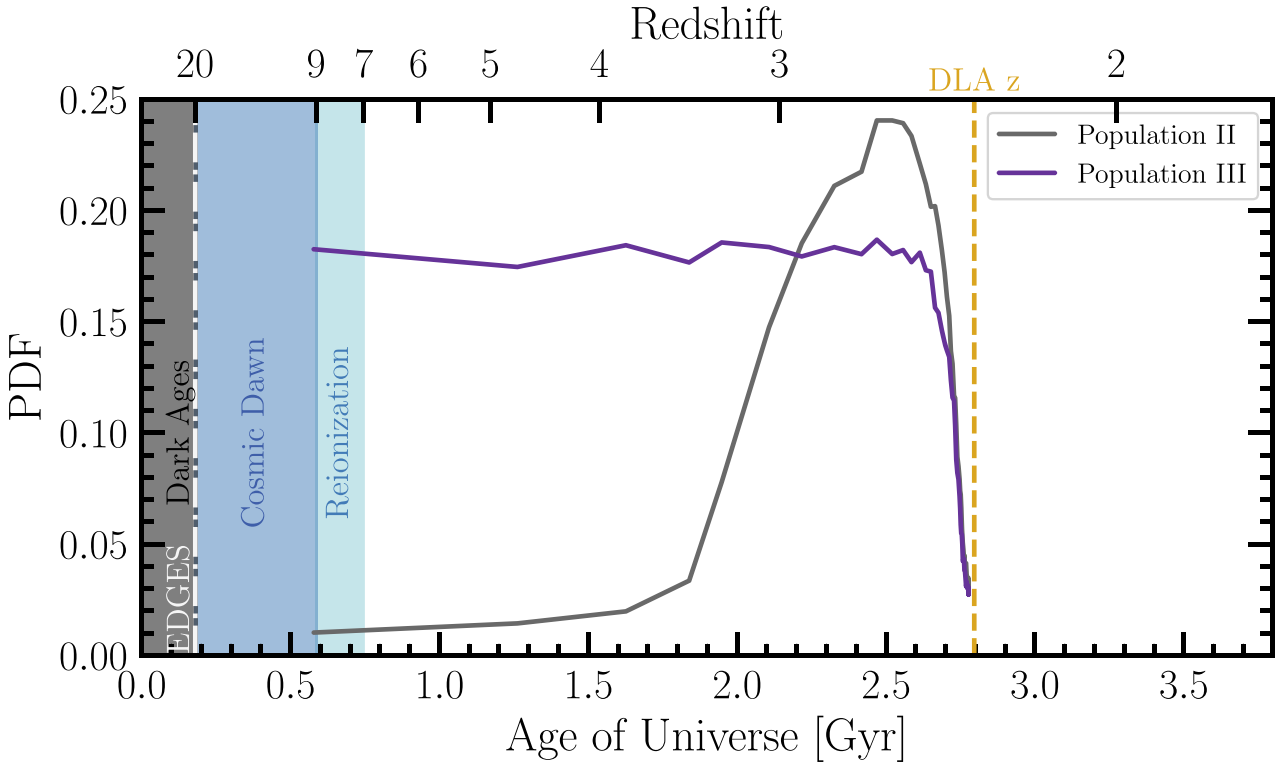

Figure 7. The most likely epoch of star formation experienced by the DLA towards J0035–0918 given our maximum likelihood enrichment model. The purple (Population III) and grey (Population II) curves indicate the probability that the stars which chemically enriched this system were born at a given redshift. A high value of the PDF indicates the most likely redshift that the DLA experienced a burst of star formation (or, equivalently, the epoch when most of the enriching stars were formed). We highlight the epoch of reionization as determined by the Planck Collaboration VI (2018) with a light-blue shaded band. Similarly, the period known as the Cosmic Dawn is shown in dark blue. Between this epoch and the Dark Ages (black shaded band) is the recent EDGES detection (vertical white dot–dashed line) from Bowman et al. (2018).

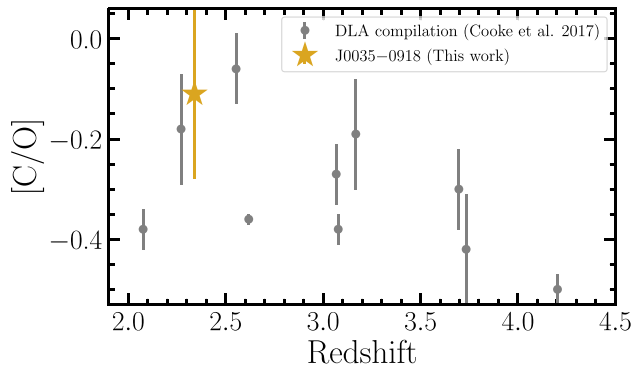

Figure 8. The redshift evolution of the measured [C/O] ratio of near-pristine DLAs. These systems are all bona fide DLAs (i.e. $\log_{10} N(\mathrm{H\,I})/\mathrm{cm}^{-2} > 20.3$) with metallicity [O/H] < -1.75 that have been observed with a high resolution ($R > 30\,000$) echelle spectrograph. The potential upward trend in [C/O] at lower redshift is supported by the [C/O] determination of J0035–0918.

redshift would mark the yields of the first low and intermediate mass Population II stars to have formed post-reionization. We may be witnessing the first tentative evidence of this effect in Fig. 8 where we plot the [C/O] abundances of the *most* metal-poor DLAs currently known as a function of their redshift. These data are based on the list compiled by Cooke, Pettini & Steidel (2017) who investigated the chemical evolution of DLAs with [O/H] < -1.75. We consider only those with $\log_{10} N(\mathrm{H\,I})/\mathrm{cm}^{-2} > 20.3$ that have also been observed with a high resolution ($R > 30\,000$) spectrograph. Fig. 8 shows tentative evidence that some near-pristine DLAs display slightly elevated [C/O] at lower redshift. We note that the size of the errors associated with each system is due to the relative saturation of the lines used to determine the abundance ratio.

4.4 Fine-structure constant

Given the quiescence and intrinsically simple cloud structure of the DLA towards J0035–0918, in combination with the wavelength stability of ESPRESSO, we have an ideal data-set for placing a bound on the invariance of the fine-structure constant α at high redshift. Given that this DLA is a near-pristine environment which is presumably living in a relatively underdense part of the Universe compared to other absorption line systems, it also offers an alternative environment to test the invariance of the fundamental couplings.

Astrophysical determinations of the variability of the fine-structure constant, $\alpha \equiv e^2/4\pi\epsilon_0\hbar c \approx 1/137$, which characterizes the strength of the electromagnetic force, has been the subject of many investigations since the advent of the 10 m class telescopes. The general principle is to measure the change of the fine-structure constant measured today (α_0) relative to a measurement at high redshift (α_z), leading to a bound of the form

$$\Delta\alpha/\alpha \equiv (\alpha_z - \alpha_0)/\alpha_0. \quad (2)$$

To obtain a measure of α_z, the observed wavelengths of several spectral lines need to be accurately measured, as each absorption

line exhibits a different sensitivity to α. This sensitivity can be parametrized by a change to the wavenumber of a given transition at high redshift, ω_z, relative to the same value measured in the laboratory today, ω_0

$$\omega_z = \omega_0 + q\,x, \tag{3}$$

where q is the sensitivity coefficient which determines how sensitive a given transition is to changes in α, and $x = (1 + \Delta\alpha/\alpha)^2 - 1$. In this work, we use the q-coefficients compiled by Berengut et al. (2011) and Murphy & Berengut (2014).

For this test, we use only the ESPRESSO data and include the absorption lines of O I λ1302, Al II λ1670, Si II λ1536, Fe II λ1608, and Fe II λ2344, which exhibit sensitivity coefficients in the range $-1165 \leq q/\mathrm{cm}^{-1} \leq 1375$. The ALIS line-fitting code that we use in our analysis includes $\Delta\alpha/\alpha$ as an optional extra parameter in the line fitting process. Specifically, ALIS reads in the atomic data (q and ω_0) of each transition, and calculates the observed wavelengths given the two model parameters (redshift and $\Delta\alpha/\alpha$). We can therefore constrain both $\Delta\alpha/\alpha$ and z simultaneously when optimizing the model profiles of the ESPRESSO data. Based on just the one absorption line system that we report here, we infer a bound on the invariance of the fine-structure constant, $\Delta\alpha/\alpha = (-1.2 \pm 1.1) \times 10^{-5}$. Given the relatively low S/N of our data owing to the faint background quasar and short integration time, this bound is impressively tight, falling just a factor of ~ 8 short of the precision achieved by Kotuš, Murphy & Carswell (2017), who reported the most precise measurement from any single absorber to date. In addition, the simplicity and quiescence of the cloud structure provides us with confidence that the modelling of the line profile has not introduced unaccounted for systematic uncertainties. We refer the reader to Murphy & Cooksey (2017) for a discussion of possible sources of uncertainty and a compilation of the most reliable results to date. The bound on $\Delta\alpha/\alpha$ that we report here is the first result that we are aware of that demonstrates the superior wavelength accuracy delivered by the ESPRESSO instrument in 4UT mode.

5 CONCLUSIONS

We report the first bound on the $^{12}C/^{13}C$ abundance ratio of a near-pristine environment using science verification data acquired with ESPRESSO in 4UT mode. Our main conclusions are as follows:

(i) We have demonstrated that the wavelength accuracy afforded by ESPRESSO permits a limit on the $^{12}C/^{13}C$ isotope ratio in the quiescent DLA towards J0035–0918 using the C II λ1334 absorption line. A significant quantity of ^{13}C, if found, could be a signature of low mass metal-free star formation.

(ii) We find that the gas cloud is well-modelled by a single absorption component whose broadening is entirely dominated by the thermal motions of the gas. On the basis of this model, we report a conservative 2σ lower limit $\log_{10}{}^{12}C/^{13}C > +0.37$. We therefore conclude that this DLA predominantly contains ^{12}C. Given this 2σ limit, we are unable to confidently rule out the presence of low-mass Population III stars at this stage.

(iii) We developed a stochastic chemical enrichment model to test whether the chemistry of this system is better modelled by Population III or Population II enrichment. We have found, given current data, that both scenarios are plausible and are equally capable of producing the observed abundances of $^{12}C/^{13}C$, [C/O], [Si/O], and [Fe/O].

(iv) Based on our best-fitting enrichment model, we estimate the DLA contains a stellar mass of $\log_{10}(M_\star/\mathrm{M}_\odot) = 4.8 \pm 1.3$ and a gas mass of $\log_{10}(M_{\mathrm{gas}}/\mathrm{M}_\odot) = 6.3^{+1.4}_{-0.9}$.

(v) We report tentative evidence that the *most* metal-poor DLA population exhibits somewhat higher [C/O] values at redshift $z \lesssim 3$. The elevated [C/O] ratios at $z \lesssim 3$ might be a signature of enrichment from the first metal-enriched low and intermediate mass stars.

(vi) Our enrichment model also suggests that – if this gas cloud is predominantly enriched by Population II stars – the bulk of the metals were produced just a few hundred Myr before the time that we observe the DLA. Prior to that, star formation in this DLA appears to have experienced a period of quiescence. We propose that this quiescence may have been caused by the cosmic reionization of hydrogen, but this can only be confirmed with future observations of near-pristine DLAs covering the redshift interval $z \simeq 2 - 4$.

(vii) We use the simplicity of the absorption profile of this system to investigate whether there is a detectable spatial or temporal variation of the fine-structure constant. When including $\Delta\alpha/\alpha$ as a free parameter in our line-fitting procedure, we find $\Delta\alpha/\alpha = (-1.2 \pm 1.1) \times 10^{-5}$.

Our work demonstrates the wealth of information made available through studying the chemistry of near-pristine absorption systems. The detailed abundance patterns of the most metal-poor DLAs provide insight into the earliest episodes of chemical enrichment. Indeed, this first bound on the C isotope ratio in a near-pristine environment has ruled out the presence of strong ^{13}C in this DLA; with data of S/N = 20, we could observationally rule out significant enrichment by low-mass Population III stars in this near-pristine environment. A similar study across the metal-poor DLA population would determine whether these systems typically show signatures of Population II or Population III enrichment. From these reconstructed enrichment histories, we may find observational evidence of reionization quenching at $2 < z < 4$ (within the redshift interval where these absorption systems are most easily studied), and be able to study the physical properties (e.g. density and temperature) of the gas affected by reionization quenching. Thanks to ESPRESSO, studies of this nature are now within the realm of possibility.

ACKNOWLEDGEMENTS

We thank the anonymous referee for providing a prompt and careful reading of the manuscript. We thank Paolo Molaro, Michael Murphy, and Dan Weisz for providing helpful comments on an earlier version of the manuscript. We are grateful to the staff astronomers at the VLT for their assistance with the observations. During this work, RJC was supported by a Royal Society University Research Fellowship. We acknowledge support from the Science and Technology Facilities Council (STFC) (ST/L00075X/1, ST/P000541/1). This project has received funding from the European Research Council (ERC) under the European Union's Horizon 2020 research and innovation programme (grant agreement No 757535). This work used the DiRAC Data Centric system at Durham University, operated by the Institute for Computational Cosmology on behalf of the STFC DiRAC High Performance Computing Facility (www.dirac.ac.uk). This equipment was funded by BIS National E-infrastructure capital grant ST/K00042X/1, STFC capital grant ST/H008519/1, and STFC DiRAC Operations grant ST/K003267/1 and Durham University. DiRAC is part of the National E-Infrastructure. This research has made use of NASA's Astrophysics Data System, and

the following software packages: Astropy (Astropy Collaboration et al. 2013), Corner (Foreman-Mackey 2016), Matplotlib (Hunter 2007), and NumPy (van der Walt, Colbert & Varoquaux 2011). Based on observations collected at the European Organisation for Astronomical Research in the Southern Hemisphere, Chile [VLT program IDs: 60.A-9508(A), 086.A-0204(A)], and the W. M. Keck Observatory [Keck program ID: A185Hb], which is operated as a scientific partnership among the California Institute of Technology, the University of California and NASA, and was made possible by the generous financial support of the W. M. Keck Foundation. We also utilize observations collected with the William Herschel Telescope [ING program ID: W/2019B/4] operated on the island of La Palma by the Isaac Newton Group of Telescopes in the Spanish Observatorio del Roque de los Muchachos of the Instituto de Astrofísica de Canarias.

REFERENCES

Abel T., Bryan G. L., Norman M. L., 2002, Science, 295, 93
Aguado D. S., Allende Prieto C., González Hernández J. I., Carrera R., Rebolo R., Shetrone M., Lambert D. L., Fernández-Alvar E., 2016, A&A, 593, A10
Akerman C. J., Carigi L., Nissen P. E., Pettini M., Asplund M., 2004, A&A, 414, 931
Allende Prieto C. et al., 2015, A&A, 579, A98
Andrievsky S. M., Spite M., Korotin S. A., Spite F., Bonifacio P., Cayrel R., François P., Hill V., 2010, A&A, 509, A88
Aoki W. et al., 2006, ApJ, 639, 897
Aoki W. et al., 2013, AJ, 145, 13
Asplund M., Grevesse N., Sauval A. J., Scott P., 2009, ARA&A, 47, 481
Astropy Collaboration, 2013, A&A, 558, A33
Barkana R., Loeb A., 2001, Phys. Rep., 349, 125
Beers T. C., Christlieb N., 2005, ARA&A, 43, 531
Beers T. C., Preston G. W., Shectman S. A., 1985, AJ, 90, 2089
Beers T. C., Preston G. W., Shectman S. A., 1992, AJ, 103, 1987
Berengut J. C., Dzuba V. A., Flambaum V. V., King J. A., Kozlov M. G., Murphy M. T., Webb J. K., 2011, Astrophys. Space Sci. Proc., 22, 9
Béthermin M. et al., 2018, A&A, 620, A115
Bond H. E., 1980, ApJS, 44, 517
Bowman J. D., Rogers A. E. E., Monsalve R. A., Mozdzen T. J., Mahesh N., 2018, Nature, 555, 67
Bromm V., Coppi P. S., Larson R. B., 2002, ApJ, 564, 23
Brown T. M. et al., 2014, ApJ, 796, 91
Bullock J. S., Kravtsov A. V., Weinberg D. H., 2000, ApJ, 539, 517
Caffau E. et al., 2013, A&A, 560, A71
Campbell S. W., Lattanzio J. C., 2008, A&A, 490, 769
Carswell R. F., Becker G. D., Jorgenson R. A., Murphy M. T., Wolfe A. M., 2012, MNRAS, 422, 1700
Cescutti G., Matteucci F., McWilliam A., Chiappini C., 2009, A&A, 505, 605
Chabrier G., 2003, PASP, 115, 763
Christlieb N., Gustafsson B., Korn A. J., Barklem P. S., Beers T. C., Bessell M. S., Karlsson T., Mizuno-Wiedner M., 2004, ApJ, 603, 708
Christlieb N., Schörck T., Frebel A., Beers T. C., Wisotzki L., Reimers D., 2008, A&A, 484, 721
Clark P. C., Glover S. C. O., Klessen R. S., Bromm V., 2011, ApJ, 727, 110
Cooke R., Pettini M., Steidel C. C., Rudie G. C., Jorgenson R. A., 2011a, MNRAS, 412, 1047
Cooke R., Pettini M., Steidel C. C., Rudie G. C., Nissen P. E., 2011b, MNRAS, 417, 1534
Cooke R. J., Pettini M., Jorgenson R. A., 2015, ApJ, 800, 12
Cooke R. J., Pettini M., Steidel C. C., 2017, MNRAS, 467, 802
Da Costa G. S. et al., 2019, MNRAS, 489, 5900
Dekker H., D'Odorico S., Kaufer A., Delabre B., Kotzlowski H., 2000, in Iye M., Moorwood A. F., eds, Proc. SPIE Conf. Ser. Vol. 4008, Optical and IR Telescope Instrumentation and Detectors. SPIE, Belligham, p. 534
Dutta R., Srianand R., Rahmani H., Petitjean P., Noterdaeme P., Ledoux C., 2014, MNRAS, 440, 307
Erni P., Richter P., Ledoux C., Petitjean P., 2006, A&A, 451, 19
Foreman-Mackey D., 2016, J. Open Source Softw., 1, 24
Foreman-Mackey D., Hogg D. W., Lang D., Goodman J., 2013, PASP, 125, 306
Frebel A. et al., 2005, Nature, 434, 871
Frebel A., Chiti A., Ji A. P., Jacobson H. R., Placco V. M., 2015, ApJ, 810, L27
Fumagalli M., O'Meara J. M., Prochaska J. X., 2011, Sci, 334, 1245
Greif T. H., Glover S. C. O., Bromm V., Klessen R. S., 2010, ApJ, 716, 510
Heger A., Woosley S. E., 2010, ApJ, 724, 341
Hirano S., Hosokawa T., Yoshida N., Umeda H., Omukai K., Chiaki G., Yorke H. W., 2014, ApJ, 781, 60
Howes L. M. et al., 2016, MNRAS, 460, 884
Hunter J. D., 2007, Comput. Sci. Eng., 9, 90
Iben I. J., 1975, ApJ, 196, 525
Karakas A. I., 2010, MNRAS, 403, 1413
Karakas A. I., 2014, MNRAS, 445, 347
Karakas A. I., Lattanzio J. C., 2014, PASA, 31, e030
Keller S. C. et al., 2007, PASA, 24, 1
Kotuš S. M., Murphy M. T., Carswell R. F., 2017, MNRAS, 464, 3679
Levshakov S. A., Centurión M., Molaro P., Kostina M. V., 2006, A&A, 447, L21
Li H.-N., Zhao G., Christlieb N., Wang L., Wang W., Zhang Y., Hou Y., Yuan H., 2015, ApJ, 798, 110
Meynet G., Hirschi R., Ekstrom S., Maeder A., Georgy C., Eggenberger P., Chiappini C., 2010, A&A, 521, A30
Morton D. C., 2003, ApJS, 149, 205
Murphy M. T., Berengut J. C., 2014, MNRAS, 438, 388
Murphy M. T., Cooksey K. L., 2017, MNRAS, 471, 4930
Nordlander T. et al., 2019, MNRAS, 488, L109
Oñorbe J., Boylan-Kolchin M., Bullock J. S., Hopkins P. F., Kereš D., Faucher-Giguère C.-A., Quataert E., Murray N., 2015, MNRAS, 454, 2092
Penprase B. E., Prochaska J. X., Sargent W. L. W., Toro-Martinez I., Beeler D. J., 2010, ApJ, 721, 1
Pepe F. A. et al., 2010, Proc. SPIE Conf. Ser. Vol. 7735, Ground-based and Airborne Instrumentation for Astronomy III. SPIE, Belligham, p. 77350F
Petitjean P., Ledoux C., Srianand R., 2008, A&A, 480, 349
Pettini M., Zych B. J., Steidel C. C., Chaffee F. H., 2008, MNRAS, 385, 2011
Planck Collaboration VI, 2018, preprint (arXiv:1807.06209)
Prantzos N., Aubert O., Audouze J., 1996, A&A, 309, 760
Robert P. F., Murphy M. T., O'Meara J. M., Crighton N. H. M., Fumagalli M., 2019, MNRAS, 483, 2736
Romano D., Karakas A. I., Tosi M., Matteucci F., 2010, A&A, 522, A32
Salpeter E. E., 1955, ApJ, 121, 161
Stacy A., Bromm V., 2014, ApJ, 785, 73
Stacy A., Bromm V., Lee A. T., 2016, MNRAS, 462, 1307
Starkenburg E. et al., 2017, MNRAS, 471, 2587
Tegmark M., Silk J., Rees M. J., Blanchard A., Abel T., Palla F., 1997, ApJ, 474, 1
Turk M. J., Abel T., O'Shea B., 2009, Science, 325, 601
van der Walt S., Colbert S. C., Varoquaux G., 2011, Comput. Sci. Eng., 13, 22
Vogt S. S. et al., 1994, in Crawford D. L., Craine E. R., eds, Proc. SPIE Conf. Ser. Vol. 2198, Instrumentation in Astronomy VIII, SPIE, Bellingham. p. 362
Webster D., Bland-Hawthorn J., Sutherland R., 2015a, ApJ, 799, L21

Webster D., Bland-Hawthorn J., Sutherland R. S., 2015b, ApJ, 804, 110
Weisz D. R. et al., 2012, ApJ, 748, 88
Weisz D. R., Dolphin A. E., Skillman E. D., Holtzman J., Gilbert K. M., Dalcanton J. J., Williams B. F., 2014, ApJ, 789, 148
Welsh L., Cooke R., Fumagalli M., 2019, MNRAS, 487, 3363
Wheeler C., Oñorbe J., Bullock J. S., Boylan-Kolchin M., Elbert O. D., Garrison-Kimmel S., Hopkins P. F., Kereš D., 2015, MNRAS, 453, 1305
Woosley S. E., 2017, ApJ, 836, 244
Woosley S. E., Weaver T. A., 1995, ApJS, 101, 181
Woosley S. E., Heger A., Weaver T. A., 2002, Rev. Mod. Phys., 74, 1015
Wright A. C., Brooks A. M., Weisz D. R., Christensen C. R., 2019, MNRAS, 482, 1176
Zafar T., Centurión M., Péroux C., Molaro P., D'Odorico V., Vlbaadilo G., Popping A., 2014, MNRAS, 444, 744

This paper has been typeset from a TEX/LATEX file prepared by the author.